# **Experimental Characterization of Heat Transfer Mechanisms in the Flow Boiling of Water on Surfaces with Engineered Micropillars**

# Chi Wang<sup>1</sup>, Md Mahamudur Rahman<sup>1,2</sup>, and Matteo Bucci<sup>1\*</sup>

Department of Nuclear Science and Engineering, Massachusetts Institute of Technology
Department of Mechanical Engineering, University of Texas at El Paso
\* mbucci@mit.edu

[leave space for DOI, which will be inserted by ANS]

## **ABSTRACT**

Surfaces with micropillars have been studied extensively and proved effective in enhancing critical heat flux (CHF) in pool boiling. However, while many studies have proposed models to explain the physical mechanisms enabling the observed CHF enhancements in pool boiling, it is still very much unclear how micropillars contributes to the CHF enhancements in pool boiling, let alone flow boiling or high-pressure conditions. Here, we conduct subcooled flow boiling experiments at operating pressures of 1 bar and 4 bar with micropillars on a newly developed heating device, which allow us to measure the time-dependent temperature and heat flux distributions on the boiling surface using high-resolution infrared thermometry. Our results confirm that square micropillars (with a width and pitch of 10 µm and a height of 10 µm) can enhance CHF in flow boiling conditions compared to a plain surface. At 1 bar, with a mass flux of 1000 kg/m<sup>2</sup>/s and a subcooling of 10 °C, the enhancement is 0.93 MW/m<sup>2</sup>. At 4 bar, with the same subcooling and mass flux, the enhancement is 1.87 MW/m<sup>2</sup>. More importantly, thanks to our temperature and heat flux distributions measurements, we show that an intra-pillar liquid layer exists among the micropillars in flow boiling. We are also able to quantify that at 1 bar, only 56% of the total CHF enhancement comes from evaporation of this liquid layer trapped within the micropillars when bubbles nucleate and grow on the heated surface. The remaining energy is removed thanks to an enhancement of forced convection and transient conduction heat transfer. The evaporation of this liquid layer plays a more important role at 4 bar due to larger area fractions occupied by evaporation regions at higher pressures.

**KEYWORDS** 

Flow boiling, micropillar, infrared thermometry, high pressure

#### 1. INTRODUCTION

Flow boiling is used in light water reactors to remove energy from the core. While it is a very effective heat transfer process that allows removing very high heat fluxes with minimum cladding-to-coolant temperature differences, it is limited by a phenomenon called a boiling crisis, which occurs if the heat flux to be removed from the surface exceeds a limit called critical heat flux (CHF). This boiling crisis may lead to the release of fission products from the cladding to the primary system. Thus, nuclear reactors are operated not to exceed the CHF limit, with large margin of conservativism. Increasing CHF limits is an intriguing opportunity. On the one hand, if the reactor power cannot be changed, higher CHF limits means higher safety margin. On the other hand, if the reactor power can be increased, higher CHF limits may enable higher reactor power and better economics (as the cost of electricity is inversely proportional to the reactor power rating), while preserving the same safety margins.

\_

<sup>\*</sup> Corresponding author.

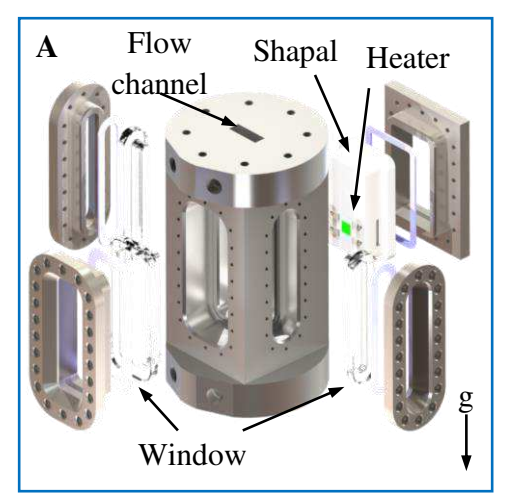
Recently, it has been found that surfaces with hydrophilic structures, e.g., porous layers [1-4], nanowires [5-7] and micropillars [8-12], can increase the CHF substantially in pool boiling. Among these structures, micropillars have been widely studied due to their well-controlled geometry and mature fabrication techniques, at least on small scale surfaces. To explain the enhancements observed on micropillars and other structures, many theories have been proposed, such as increased roughness factor [8], evaporation of wicking flow [9], facilitated re-wetting [10] and evaporation of retention liquid [13]. However, no direct experimental evidence has been obtained for these hypotheses until very recently a study from our group showed that the pool boiling CHF enhancement on micropillars comes from the evaporation of an intrapillar liquid layer as well as the increased heat transfer in the non-evaporation region, i.e., forced convection and transient conduction [12].

Although our recent work shed some light on the mechanisms of CHF enhancements in pool boiling, it is unclear if these mechanisms (i.e., existence and evaporation of the intra-pillar liquid layer, increased forced convection and transient conduction) persist in flow boiling conditions, where the bubble dynamics is driven by the presence of flow field and pressurization, if any. In addition, studies about CHF enhancements in flow boiling are mainly focused on refrigerants [14]. Most of the available flow boiling studies with water have been carried out in microscale flow channels [15] and the conclusions cannot be directly applied to nuclear industry with macroscale flow channels. To fill this knowledge gap, we conduct flow boiling experiments with micropillar surfaces at different pressures in flow channels that are comparable to those used in nuclear power plants. We use a specially designed heater and infrared (IR) thermometry to obtain time-dependent measurements of the temperature and heat flux distributions on micropillar surfaces. Based on these measurements, we show the existence of the intra-pillar liquid layer in flow boiling, which is similar to what we have found in pool boiling. We also find that evaporation of this intra-pillar liquid layer contributes to roughly 56% of the total CHF enhancement compared to a plain surface, which is higher than the 30% we measured in pool boiling. Also, and importantly, the enhancement increases with pressure.

# 2. Experimental Facilities and Heater design

## 2.1. High-pressure Flow Boiling Loop

Flow boiling tests are conducted in a test section shown in Fig. 1 (A), which is installed in a flow loop sketched in Fig. 1 (B). The flow channel has a rectangular cross section of 1 × 3 cm<sup>2</sup>. The external sides of test section form a square cross-section prism. Each side has an opening. Three of these openings accommodate quartz windows, which provide optical access to the flow channel. The fourth opening accommodate a ceramic cartridge made of Shapal (a ceramic material), which, in turn, accommodate the IR heater (installed vertically). Quartz windows, Shapal cartridge and IR heater are perfectly flushed with the internal walls of the flow channel. The test section is forerun by a flow channel with the same identical cross section. Such channel is longer than 60 hydraulics diameters and allows to reach fully developed flow conditions in correspondence of the IR heater. Water flows upward. At the inlet and outlet of the test section, pressure and temperature are monitored. Two sets of pre-heaters (i.e., heat tapes) are installed along the flow loop to heat the flow to desired temperature. A flow meter is installed between the pump outlet and test section inlet to measure the volumetric flow rate, which is then converted into mass flux in the test section. The flow loop, with exception of the test section, is wrapped by insulation material to minimize heat losses to the external environment. The thermal balance of the loop is completed by a heat exchanger cooled by a chilled water line. More details about test section, flow loop, and instrumentation can be found in Refs. [16, 17]. During the tests, the IR radiation emitted by the heater is reflected by a mirror to an IR camera (Telops M3k). The recorded radiation is post processed to get the temperature and heat flux distributions using techniques described in Ref. [18].



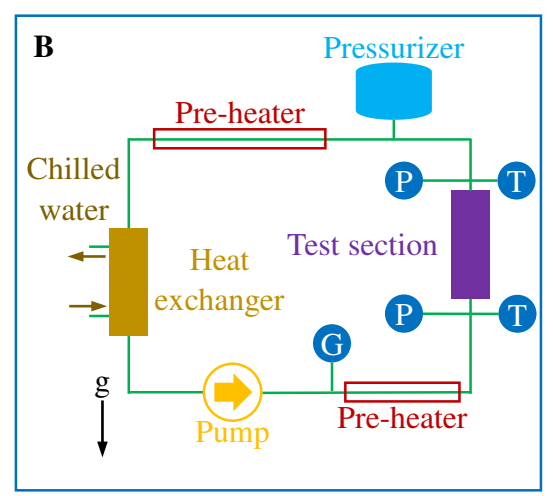


Figure 1. The test section is shown in (A) and the diagram of the entire loop is illustrated in (B), where 'P' and 'T' represent the pressure sensors and thermocouples.

Before the tests, the flow loop is filled with deionization (DI) water. Then, the DI water is circulated through a degassing membrane to remove non-condensable gases. Once the degassing is completed, the DI water is heated to desired temperature, e.g., 90 °C at 1 bar, using the pre-heaters and stabilized using the heat exchanger. After the flow temperature is stabilized, a moderate voltage is applied to the heater to generate bubbles on the boiling surface and remove non-condensable gases trapped on the boiling surface. Then, the voltage applied to the heater is increased in small steps, until the boiling crisis occurs. The signature of the boiling crisis is a rapid escalation of the heater temperature, which is captured by the IR camera. Such rapid temperature escalation may break the heater. Thus, when the boiling crisis occurs, we immediately shut down the power to save the heater. This task is accomplished by a special burnout prevention system, discussed in Ref. [17].

The flow boiling tests are run with a subcooling of 10 K and a mass flux of 1000 kg/m²/s. Tests are conducted at two different pressures, i.e., 1 bar and 4 bar. The current and voltage are recorded at a frequency of 10000 Hz. The IR camera records at 3000 frames per second (FPS). At each time step, the IR camera and the data acquisition system for heater current and voltage start recording at the same time and take measurements for about 2 seconds.

#### 2.2. Heater Fabrication and Characterization

The heater used in this work, as illustrated in Fig. 2, features a multi-layer structure fabricated on a 1 mm thick sapphire substrate by techniques used for micro-electromechanical systems (MEMS). The heater with hydrophilic micropillars is shown in Fig. 2 (A). We also used a heater with a plain "reference" surface, shown in Fig. 2 (B), as a term of comparison. Heat is generated by joule heating in the 1  $\mu$ m thick chromium (Cr) layer on top of the sapphire substrate. The active heat area, which is 10 mm × 10 mm, is defined by covering the Cr heating layer with sliver (Ag) pads at two sides and leaving an uncovered center part. During tests, voltage is applied on the silver pads to create a current flowing through the Cr heating layer. The 4  $\mu$ m thick alumina (Al<sub>2</sub>O<sub>3</sub>) layer between the Cr heating layer and the electroplated copper pillar functions as an electrical insulation layer. The top Cr layer is used to cover the copper pillars to prevent them from oxidization during boiling tests. All the different layers are deposited by sputtering and atomic layer deposition (ALD) while the micropillars are obtained by electroplating copper in a polymer mold fabricated using photolithography. All the fabrication processes are carried out in the clean rooms at the MIT Nano facility. More details about the fabrication process can be found in Ref. [19].

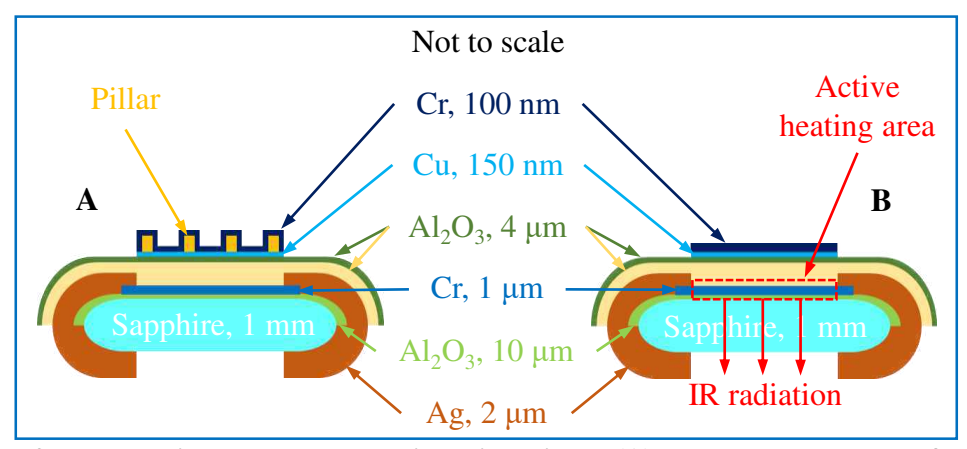


Figure 2. The multi-layer IR heater with micropillars (A) and nano-smooth surface (B).

The micropillars are designed to be square with a size of  $10 \times 10 \ \mu m^2$  and a height of  $10 \ \mu m$ . After fabrication, the actual size and height of the pillars are measured to be  $8.94 \times 10.60 \ \mu m^2$  and  $9.40 \ \mu m$ , respectively, according to scanning electron microscope (SEM) images shown in Fig. 3.

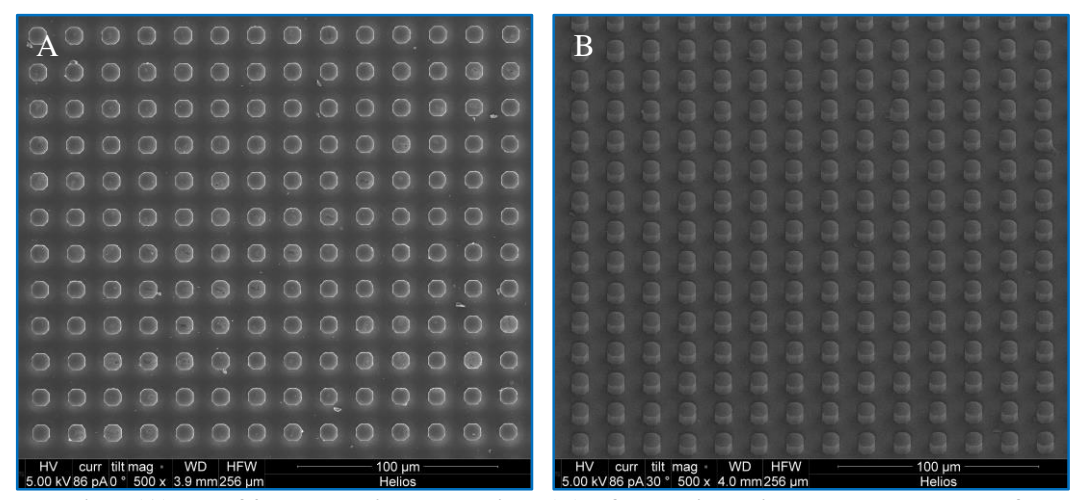


Fig. 3. Top view (A) and 30-degree tilt angle view (B) of the micropillars. The corners of the square pillars are not well plated during electroplating, but the shape is roughly square.

The micropillar surface exhibits super hydrophilic properties in wicking test. The apparent contact angle is practically 0 degree. Following the droplet spreading test proposed in Ref. [20] and wicking test proposed in Ref. [9], the average permeability of the micropillars are measured to be  $2.55 \times 10^{-12}$  m<sup>2</sup> and wicking number of the micropillar surface is measured to be 0.82. The nano-smooth surface is a plain surface with a roughness (Sa) smaller than 10 nm and a contact angle around 30 degree. More details about the droplet spreading test, the wicking test, roughness and contact angle measurement on the plain surface can be found in Refs. [12, 19].

#### 3. Results and Discussions

The boiling curves at 1 bar and 4 bar are plotted in Fig. 4 (A) and Fig. 4 (B), respectively. As we can see, the pillar surface can enhance the CHF at both pressures. In particular, the CHF is 3.15 MW/m² on the plain surface and 4.08 MW/m² on the engineered surface at 1 bar. The CHF enhancement is 30% (i.e., 0.93 MW/m²). At 4 bar, the CHF is 3.58 MW/m² on the plain surface and 5.45 MW/m² on the engineered surface. The CHF enhancement at 4 bar is thus 52% (i.e., 1.87 MW/m²). The enhancements at both pressures are

smaller than the predictions based on the wicking number, i.e., 100%, which suggests that the wicking model developed for pool boiling experiments by Rahman et al. [9], is not directly applicable in flow boiling.

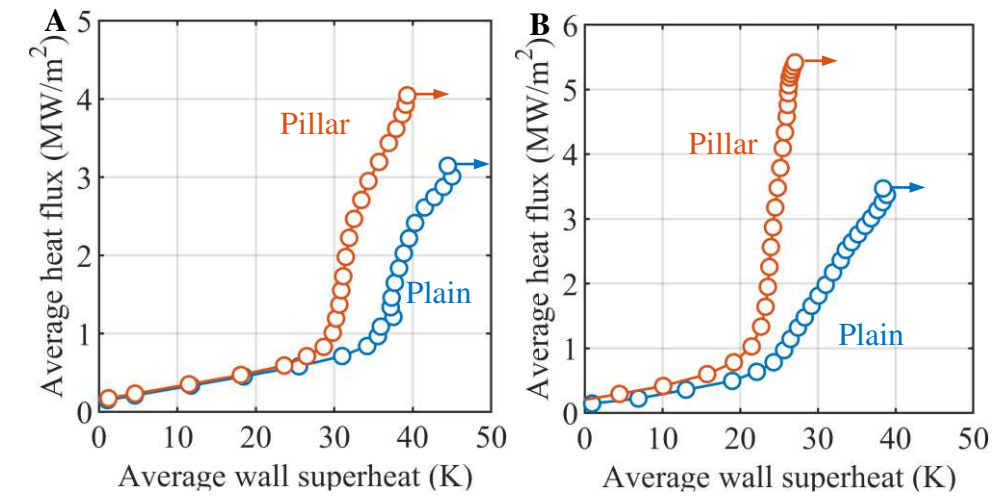


Figure 4. Flow boiling curves at 1 bar (A) and 4 bar (B). The arrows represent the last steady state before the boiling crisis.

Figure 5 shows the heat flux distributions for the plain surface (A) and pillar surface (B) at 1 bar. We can see high heat flux regions (red color in Fig. 5) corresponding to evaporation of the microlayer on the lain surface (A). As the microlayer dries out, the surface gets covered by vapor, with poor heat transfer properties. This occurs because the microlayer under bubbles is very thin and dries very quickly. However, on the pillar surface, strong evaporation occurs consistently all over the area covered by bubbles, which does not dry out. This behavior indicates the existence of an intra-pillar liquid layer which is much thicker than the microlayer on the plain surface [12].

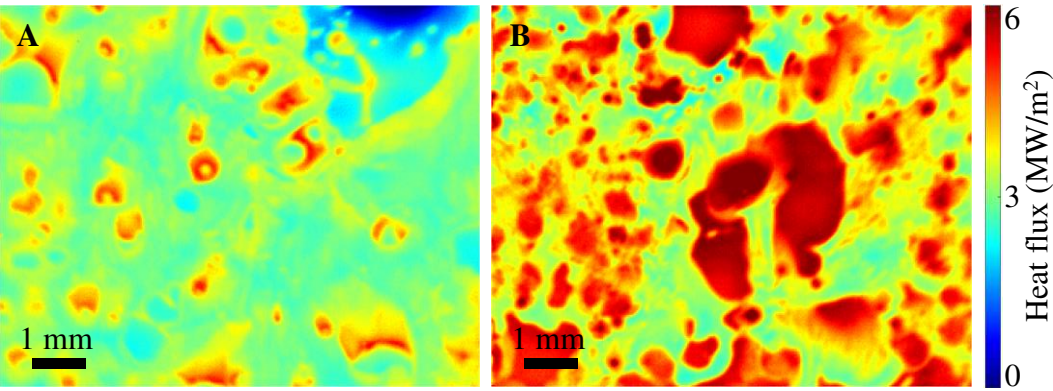


Figure 5. Distributions of heat flux in flow boiling tests at 1 bar on the plain surface (A), where the average heat flux is 3.15 MW/m<sup>2</sup>, and the pillar surface (B), where the average heat flux is 4.05 MW/m<sup>2</sup>.

The evaporation of this intra-pillar liquid layer is more evident in the bivariate histograms shown in Fig. 6. We can see there is only one peak, which is the nucleate boiling peak, in the bivariate histograms for the plain surface shown in Fig. 6 (A). For the pillar surface, the bivariate histograms, plotted in Fig. 6 (B), shows two peaks, i.e., the nucleate boiling peak and the peak due to the evaporation of the intra-pillar liquid layer.

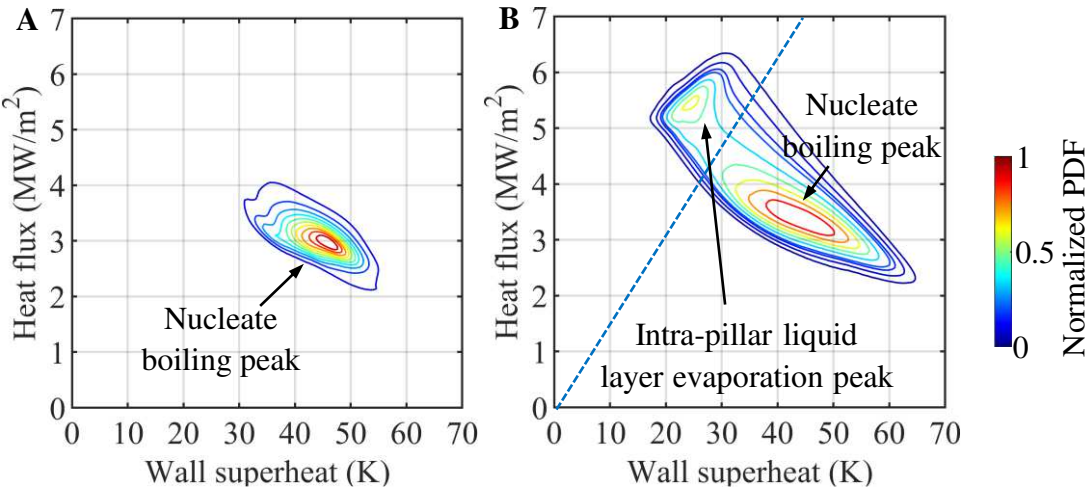


Figure 6. Bivariate histograms in flow boiling at 1 bar on the plain surface (A), where the average heat flux is 3.15 MW/m<sup>2</sup>, and on the pillar surface (B), where the average heat flux is 4.05 MW/m<sup>2</sup>.

With this intense evaporation of the intra-pillar liquid layer, one may be tempted to conclude that the evaporation of this liquid layer is the mechanism enabling CHF on the pillar surfaces. However, it is only one of the reasons. Hereafter, we show heat flux partitioning measurements. The two peaks in the bivariate histograms of the pillar surface shown in Fig. 6 (B) indicate two different heat transfer mechanisms. In the region of the bivariate histogram labelled "intra-pillar liquid layer evaporation peak," heat is removed from the surface by evaporation of the liquid. In the "nucleate boiling peak" region, instead, it is found that the main heat transfer mechanisms are related to non-phase-change heat transfer, i.e., forced convection and transient conduction [12]. Therefore, we can quantify how much heat is removed by evaporation and non-evaporative (singe-phase) mechanisms by separating the two peaks using the dashed line shown in Fig. 6 (B). A detailed demonstration of this technique can be found in Refs. [12, 19]. Doing this, we get the results plotted in Fig. 7.

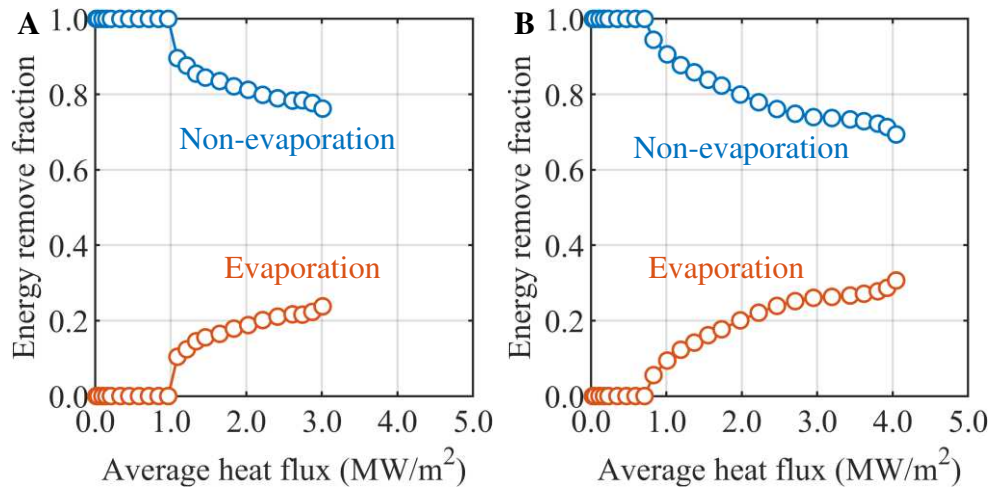


Figure 7. Heat flux partition in flow boiling at 1 bar for the plain surface (A) and for the pillar surface (B).

As we can see from Fig. 7 (A), the fraction of energy removed by the evaporation region is around 24% at the boiling crisis on the plain surface, which is equivalent to 0.77 MW/m<sup>2</sup>. Figure 7 (B) shows that the fraction of energy removed by the evaporation region on the pillar surface is 31%, which is equivalent to

 $1.26~\mathrm{MW/m^2}$ . If we only compare the equivalent heat flux of the energy removed by evaporation, there is an increase of  $0.49~\mathrm{MW/m^2}$ , which is less than the CHF enhancement on the pillar surface,  $0.87~\mathrm{MW/m^2}$ . The energy removed by the non-evaporation region increases by  $0.38~\mathrm{MW/m^2}$ , which is slightly smaller than the increase in the evaporation region.

Based on this, we can conclude that the CHF enhancement on the pillar surface comes from the increase of both the evaporation region and non-evaporation region heat transfer. The evaporation of the intra-pillar liquid layer itself cannot explain the entirety of the CHF enhancement. These conclusions are very similar to what we have found in pool boiling [12].

Although its evaporation is not enough to account for the CHF increase, the intra-pillar liquid layer still plays a crucial role in CHF enhancement in flow boiling at 1 bar by delaying the boiling crisis and enabling the heat transfer mechanisms to continue their function at higher average heat flux, as demonstrated by Fig. 8 which shows the average heat flux in each region and the area occupied by the evaporation region.

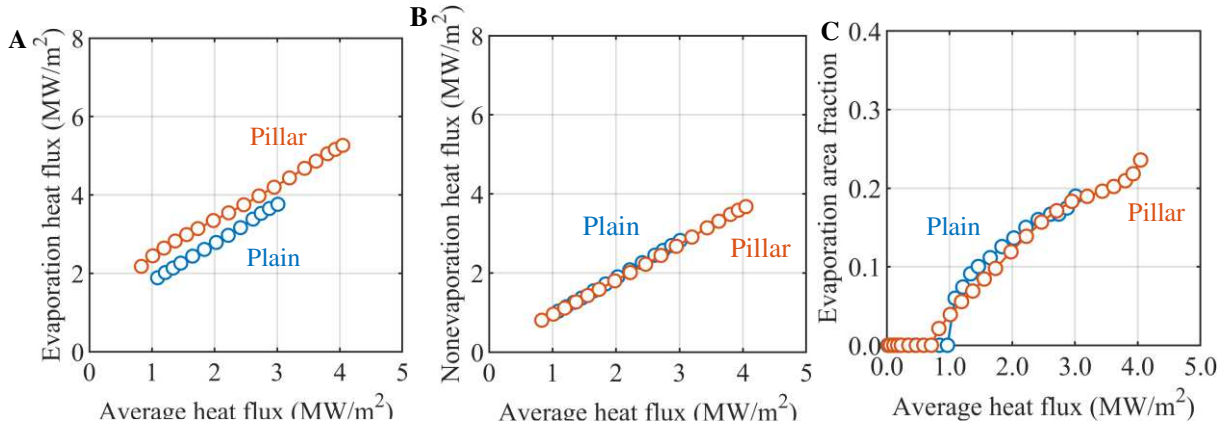


Figure 8. Normalized heat flux in the evaporation region (A) and non-evaporation region (B) for flow boiling at 1 bar. Fraction of area occupied by evaporation region (C).

We can see from Fig. 8 (A) and Fig. 8 (B) that at the same average heat flux, in both the evaporation region and the non-evaporation region, the pillar surface and the plain surface have very similar heat fluxes. Although the evaporation of the intra-pillar liquid layer appears to be very intense from the heat flux distribution shown in Fig. 5 (B), the average heat flux in the evaporation region on the pillar surface is only slightly higher than that on the plain surface, as shown by Fig. 8 (A). In addition, Fig. 8 (C) shows that the evaporation areas on the two surfaces are also very close at the same average heat flux. So, if the bubble configurations on the pillar surface create an irreversible dry patch at around 3 MW/m², the pillar surface would have the same CHF as the pillar surface. However, the irreversible dry patch that leads to the boiling crisis is delayed to around 4 MW/m² on the pillar surface due to the existence of the intra-pillar liquid layer. This delay makes it possible for the heat transfer mechanisms in the evaporation region and non-evaporation region continue remove heat. Therefore, the intra-pillar liquid layer, by keeping the pillar surface soaked with water, is the major reason for the increased heat flux in the evaporation region, in the non-evaporation region at the boiling crisis, and thus for the increase CHF.

While the existence of the intra-pillar liquid layer on the pillar surface is evident in flow boiling at 1 bar, it becomes relatively less observable at higher pressures, i.e., 4 bar, due to smaller bubble sizes and limitations of the spatial and temporal resolutions of the IR camera. Figure 9 shows the heat flux distribution of the two surfaces at 4 bar.

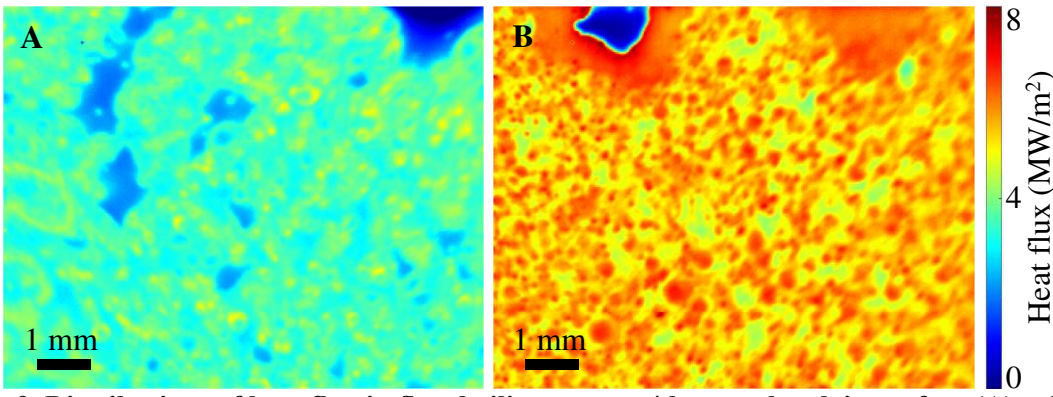


Figure 9. Distributions of heat flux in flow boiling tests at 4 bar on the plain surface (A), where the average heat flux is  $3.52 \text{ MW/m}^2$ , and on the pillar surface (B), where the average heat flux is  $5.42 \text{ MW/m}^2$ .

We can still observe more intense evaporation and less dry patches from the heat flux on the pillar surface shown in Fig. 9 (B) comparing the plain surface shown in Fig. 9 (A), which is a strong indication of the intra-pillar liquid layer. However, more direct evidence, such as the evaporation peak of the intra-pillar liquid layer, are not visible in the bivariate histograms, as shown in Fig. 10.

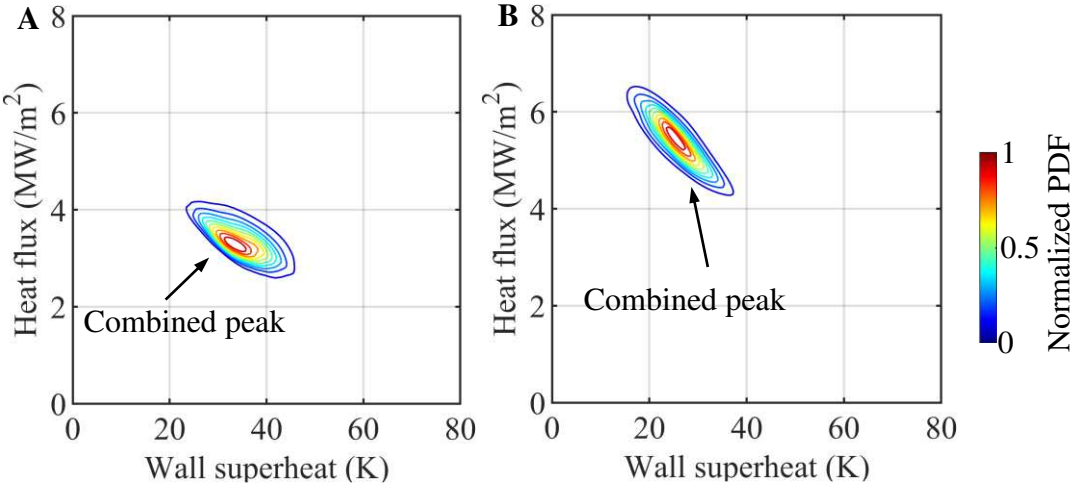


Figure 10. Bivariate histograms in flow boiling at 4 bar for the plain surface (A), where the average heat flux is 3.52 MW/m<sup>2</sup> and the pillar surface (B), where the average heat flux is 5.42 MW/m<sup>2</sup>.

We can see from Fig. 10 that only one peak is visible for both the plain surface and the pillar surface at 4 bar. We think the intra-pillar liquid layer still exist at 4 bar. However, capturing its evaporation process and revealing its effect becomes much more difficult at high pressures because the bubbles are much smaller and faster. Future studies with faster and better-resolution IR cameras are needed to confirm our hypothesis.

# 4. CONCLUSIONS

In this work, we study subcooled flow boiling CHF enhancement using nano-engineered surfaces, i.e., super hydrophilic micropillars. To do this, we design and use a special IR heater with micropillars, which enables direct measurement of temperature and heat flux distributions using IR thermometry. To the best of the authors' knowledge, it is the first time such measurements have been achieved on micropillar surfaces in subcooled flow boiling. Based on our measurements, we can conclude that:

- 1. The micropillar surfaces enhance the flow boiling CHF at ambient pressure as well as higher pressure (e.g., 4 bars). The primary reason for the enhancement is the presence of an intra-pillar liquid layer, which delays the appearance of dry patches that lead to boiling crisis.
- 2. Evaporation of the intra-pillar liquid layer is not the only mechanism that contributes to the increased CHF. Heat transfer mechanisms in the non-evaporation region, i.e., forced convection and transient conduction, contribute to the same extent as evaporation to the CHF enhancement in flow boiling.
- 3. The intra-pillar liquid layer becomes more difficult to identify at 4 bar due to smaller and faster bubbles. However, intense evaporation and rare dry patches in the heat flux distributions on micropillar surfaces at 4 bar strongly indicate its existence.

In the future, we will investigate the effects of different micropillars on CHF enhancements in subcooled flow boiling at different working conditions, e.g., different pressures, mass fluxes and subcooling.

#### **ACKNOWLEDGMENTS**

The results presented in this paper were obtained in research projects sponsored by the National Science Foundations and the Exelon Corporation through its membership in the MIT Energy Initiative.

#### REFERENCES

- 1. H. D. Kim, and M. H. Kim, "Effect of nanoparticle deposition on capillary wicking that influences the critical heat flux in nanofluids," *Appl. Phys. Lett.* **91**(1), pp. 014104 (2007).
- 2. S. Li, R. Furberg, M. S. Toprak, B. Palm, and M Muhammed, "Nature-inspired boiling enhancement by novel nanostructured macroporous surfaces," *Adv. Funct. Mater.* **18**(15), pp. 2215-2220 (2008).
- 3. M. Tetreault-Friend et al., "Critical heat flux maxima resulting from the controlled morphology of nanoporous hydrophilic surface layers," *Appl. Phys. Lett.* **108**(24) pp. 243102 (2016).
- 4. C. Wang et al., "Investigation of CHF Enhancement on Nanoengineered Surfaces in Pressurized Subcooled Flow Boiling using Infrared Thermometry," *Heat Transf. Eng.* Pp. 1-25 (2023).
- 5. C. Li et al., "Nanostructured copper interfaces for enhanced boiling," Small 4(8) pp. 1084-1088 (2008).
- 6. R. Chen et al., "Nanowires for enhanced boiling heat transfer," *Nano Lett.* **9**(2), pp. 548-553 (2009).
- 7. M. M. Rahman, E. Ölçeroğlu, and M. McCarthy, "Scalable nanomanufacturing of virus-templated coatings for enhanced boiling," *Adv. Mater. Interfaces* **1**(2) pp. 1300107 (2014).
- 8. K. H. Chu, R. Enright, and E. N. Wang, "Structured surfaces for enhanced pool boiling heat transfer," *Appl. Phys. Lett.* **100**(24) pp. 241603 (2012).
- 9. M. M. Rahman, E. Olceroglu, and M. McCarthy, "Role of wickability on the critical heat flux of structured superhydrophilic surfaces," *Langmuir* **30**(37) pp. 11225-11234 (2014).
- 10. N. S. Dhillon, J. Buongiorno, and K. K. Varanasi. "Critical heat flux maxima during boiling crisis on textured surfaces," *Nat. Commun.* **6**(1) pp. 1-12 (2015).
- 11. D. E. Kim, S. C. Park, D. I. Yu, M. H. Kim, and H. S. Ahn, "Enhanced critical heat flux by capillary driven liquid flow on the well-designed surface," *Appl. Phys. Lett.* **107**(2), pp. 023903 (2015).
- 12. C. Wang, M. M. Rahman and M. Bucci, "Decrypting the Mechanisms of Wicking and Evaporation Heat Transfer on Micro-pillars during the Pool Boiling of Water Using High-resolution Infrared Thermometry", *Phys. Of Fluids* 35(3) pp. 037112 (2023).
- 13. J. Li et al., "Liquid film-induced critical heat flux enhancement on structured surfaces," *Sci. Adv.* 7(26) pp. eabg4537 (2021).

- 14. G. Liang, and I. Mudawar, "Review of channel flow boiling enhancement by surface modification, and instability suppression schemes," *Int. J. Heat Mass Transf.* **146** pp.118864 (2020).
- 15. D. Li et al., "Enhancing flow boiling heat transfer in microchannels for thermal management with monolithically-integrated silicon nanowires," *Nano Lett.* **12**(7) pp.3385-3390 (2012).
- 16. A. Richenderfer et al., "Investigation of Subcooled Flow Boiling and CHF Using High-Resolution Diagnostics," *Exp. Therm. Fluid Sci.* **99** pp.35-58 (2018).
- 17. A. Richenderfer, *Experimental Study of Heat Flux Partitioning in Pressurized Subcooled Flow Boiling*, Doctoral dissertation, Massachusetts Institute of Technology (2018).
- 18. M. Bucci, A. Richenderfer, G. Su, T. McKrell and J. Buongiorno, "A mechanistic IR calibration technique for boiling heat transfer investigations" *Int. J. Multiph. Flow* **83** pp.115-127 (2016).
- 19. C. Wang, Experimental Investigation of Critical Heat Flux Enhancement on Engineered Surfaces with Infrared Thermometry, Doctoral dissertation, Massachusetts Institute of Technology (2022).
- 20. C. K. Wemp and V. P. Carey, "Water wicking and droplet spreading on randomly structured thin nanoporous layers," *Langmuir* **33**(50), pp.14513-14525 (2017).